

Differential ripple propagation along the hippocampal longitudinal axis

Roberto De Filippo¹ and Dietmar Schmitz¹²³⁴⁵

¹ Charité Universitätsmedizin Berlin, corporate member of Freie Universität Berlin, Humboldt-Universität zu Berlin, and Berlin Institute of Health; Neuroscience Research Center, 10117 Berlin, Germany.

² German Center for Neurodegenerative Diseases (DZNE) Berlin, 10117 Berlin, Germany.

³ Charité-Universitätsmedizin Berlin, corporate member of Freie Universität Berlin, Humboldt-Universität Berlin, and Berlin Institute of Health, Einstein Center for Neuroscience, 10117 Berlin, Germany.

⁴ Charité-Universitätsmedizin Berlin, corporate member of Freie Universität Berlin, Humboldt-Universität Berlin, and Berlin Institute of Health, NeuroCure Cluster of Excellence, 10117 Berlin, Germany.

⁵ Humboldt-Universität zu Berlin, Bernstein Center for Computational Neuroscience, Philippstr. 13, 10115 Berlin, Germany.

* Correspondence to: roberto.de-filippo@charite.de and dietmar.schmitz@charite.de

Keywords: Hippocampal ripples, Ripples propagation

Abstract

Hippocampal ripples are highly synchronous neural events critical for memory consolidation and retrieval. A minority of strong ripples has been shown to be of particular importance in situations of increased memory demands. The propagation dynamics of strong ripples inside the hippocampal formation are, however, still opaque. We analyzed ripple propagation within the septal half of the hippocampal formation in an open access dataset provided by the Allen Institute. Surprisingly, strong ripples propagate differentially in the septal and temporal direction along the hippocampal longitudinal axis. The septal hippocampal pole is able to generate longer ripples that engage more neurons and elicit spiking activity for an extended time along the entire septal half of the hippocampal formation. Ripples generated septally have therefore higher chances of retaining their strength while travelling within the hippocampus. Moreover, a substantial portion of the variance in strong ripple duration ($R^2 = 0.463$) is explained solely by the ripple generation point on the longitudinal axis. Our results are consistent with a possible distinctive role of the hippocampal septal pole in conditions of high memory demand.

33 Introduction

34 Hippocampal ripples are brief oscillatory events detected in the local field potential (LFP) of
35 the hippocampal formation, these events correspond to the synchronized depolarization of a
36 substantial number of neurons in various hippocampal subregions (Hulse et al., 2016, Ylinen
37 et al., 1995). An higher ripple incidence during memory encoding is associated with superior
38 recall performance (Norman et al., 2019), furthermore, ripple incidence is increased during
39 successful memory retrieval (Vaz et al., 2019, Carr et al., 2011). Ripples are also involved in
40 memory consolidation both in awake and sleep conditions (Jadhav et al., 2012, Roux et al.,
41 2017, Sirota et al., 2003, Girardeau et al., 2009), disrupting awake ripples during learning
42 causes a persisting performance degradation, the same effect can be achieved by silencing
43 ripples during post-learning sleep. Accordingly, ripples are considered to play a crucial role in
44 memory processes and reorganization of memory engrams (Girardeau and Zugaro, 2011,
45 Buzsáki, 2015, Diba and Buzsáki, 2007, Foster and Wilson, 2006, Xu et al., 2019, Takahashi,
46 2015, Davidson et al., 2009, Pfeiffer and Foster, 2015, Dragoi and Tonegawa, 2011, Girardeau
47 et al., 2009). Ripples duration exhibits a skewed distribution with only a minority of long-
48 duration ripples (> 100 ms). Interestingly, the fraction of long-duration ripples is increased in
49 novel contexts, in memory-demanding tasks and during correct recalls (Fernández-Ruiz et al.,
50 2019). Reducing ripple duration artificially causes a degraded working memory performance
51 (Jadhav et al., 2012) and, on the contrary, prolongation has a beneficial effect (Fernández-
52 Ruiz et al., 2019). Ripple duration is directly proportional to ripple amplitude (Patel et al., 2013),
53 therefore, these results point at a specific role of stronger ripples in situations of high
54 mnemonic demand and are consistent with a possible power law distribution where a minority
55 of ripples is responsible for a substantial part of memory requirements. For this reason, it is
56 of interest to identify the possible electrophysiological peculiarities of this subgroup of ripples.
57 Do strong ripples propagate differently compared to common ripples? Are strong ripples
58 generated homogeneously along the hippocampal longitudinal axis? Do ripples have a
59 preferred longitudinal directionality? In this study we focused our attention on ripples
60 generation and propagation within the hippocampal formation. Hippocampal connectivity with
61 cortical and sub-cortical areas varies considerably along the longitudinal axis (Moser and
62 Moser, 1998, Faselow and Dong, 2010) and gene expression, as well, exhibits both gradual
63 and discrete transitions along the same axis (Vogel et al., 2020, Strange et al., 2014).
64 Consequently, the hippocampus is considered to be functionally segmented along its long
65 axis. The different connectivity contributes to explain the functional organization gradient
66 between a predominantly spatio-visual (septal pole) and emotional (temporal pole)

67 processing. Ripples generated in the septal and temporal hippocampal pole have already
68 been shown to be temporally independent and able to engage different neuron
69 subpopulations, even in the same downstream brain area (Sosa et al., 2020). Consequentially,
70 a heterogeneous ripple generation chance along the longitudinal axis most probably has an
71 impact on the frequency with which different brain areas and neurons subgroups are activated
72 by ripples. Our work is based on a dataset provided by the Allen Institute (Siegle et al., 2021),
73 this dataset enabled us to study comprehensively ripples features across the septal half of
74 the hippocampus. Previous studies have looked at ripple propagation along the longitudinal
75 axes of the hippocampus (Patel et al., 2013, Kumar and Deshmukh, 2020), however, the size
76 of this dataset made it possible to unveil propagation details previously overlooked.

77 **Results**

78 **Distance explains most of the ripple strength correlation variability.**

79 We studied ripple propagation along the hippocampal longitudinal axis in an open-access
80 dataset provided by the Allen Institute. We analyzed the LFP signals across the visual cortex,
81 hippocampal formation and brain stem (Supplementary Figure 1) simultaneous to ripples
82 detected in the CA1 of 49 animals (average session duration = 9877.4 ± 43.1 seconds, average
83 ripple incidence during non-running epochs = 2.49 ± 0.12 per 10s). Ripples (n ripples =
84 120462) were detected on the CA1 channel with the strongest ripple activity. Ripple strength
85 (J_{Ripple}) was calculated as the integral of the filtered LFP envelope between the start and end
86 points for every detected ripple (Supplementary Figure 2b). Clear ripples were observed
87 uniquely in the hippocampal formation (CA1, CA2, CA3, DG, SUB, ProS). Likewise, ripple-
88 induced voltage deflections (RIVD, integral of the unfiltered LFP envelope) were also
89 noticeably stronger in hippocampal areas (Supplementary Figure 2c-f). Ripple strength was
90 noticeably irregular in single sessions both across time and space, even within the CA1 region
91 (Supplementary Figure 2c). We focused on the variability in ripple strength across pairs of CA1
92 recording locations with clear ripple activity (n CA1 pairs = 303, n sessions = 46). Correlation
93 of ripple strength across different CA1 regions was highly variable (Figure 1a-b-c) with a lower
94 and upper quartiles of 0.66 and 0.87 (mean = 0.76, SEM = 0.01). Distance between recording
95 location could explain the majority (57.6%) of this variability (Figure 1b) with the top and
96 bottom quartiles of ripple strength correlation showing significantly different average
97 distances (Figure 1c-d). Given the correlation variability we asked how reliably a ripple can
98 travel along the hippocampal longitudinal axis. To answer this question, we looked at ripples

99 lag in sessions that included both long-distance ($> 2126.66 \mu\text{m}$) and short-distance (< 857.29
100 μm) CA1 recording pairs (n sessions = 32, n CA1 pairs = 64, Figure 1e). Reference for the lag
101 analysis was always the most medial recording location in each pair. Almost half of the ripples
102 in long-distance pairs ($49.3 \pm 2.2\%$) were detected in both locations (inside a 120 ms window
103 centered on ripple start at the reference location). Unsurprisingly short-distance pairs showed
104 a more reliable propagation ($69.59 \pm 3.51\%$). Moreover, lag between long-distance pairs had
105 a much broader distribution (Figure 1f) and a significantly bigger absolute lag (Figure 1g).
106 Neither high nor short-distance pairs showed clear directionality (lag long-distance = $-1.14 \pm$
107 0.64 ms, lag short-distance = -0.5 ± 0.41 ms). Looking at the relationship between lag and
108 ripple strength in long-distance pairs, however, an asymmetric distribution was apparent
109 (Figure 1f top), suggestive of a possible interaction between these two variables: stronger
110 ripples appear to be predominantly associated with positive lags (i.e. ripples moving
111 medial→lateral). To further investigate this relationship we divided ripples into two groups:
112 strong (top 10% ripple strength per session at the reference location) and common (remaining
113 ripples). The septal half of the hippocampus was divided in three sections with equal number
114 of recordings: medial, central and lateral (Supplementary Figure 3). Strong ripples identified in
115 the medial section, in opposition to common ripples, showed a markedly positive lag (lag =
116 17.83 ± 1.02 ms) indicative of a preferred medial→lateral travelling direction (Figure 1h top).
117 Surprisingly, the same was not true for strong ripples identified in the lateral section (lag =
118 3.62 ± 1.05 ms, Figure 1i). Strong and common ripples lags were significantly different
119 between medial and lateral locations both in common and strong ripples. A biased direction
120 of propagation can be explained by an unequal chance of ripple generation across space. We
121 can assume that selecting strong ripples we are biasing our focus towards ripples whose
122 generation point (seed) is situated nearby our reference location, this would contribute to
123 explain the unbalanced lag. This notion would, however, fail to explain the different
124 directionality we observed between strong ripples in medial and lateral locations. This hints
125 at a more complex situation.

126 **Ripples propagates differentially along the hippocampal longitudinal axis.**

127 To analyze the propagation of ripples along the hippocampal longitudinal axis we focused on
128 sessions from which ripples were clearly detected in at least two different hippocampal
129 sections at the same time ($n = 41$). We followed the propagation of strong and common ripples
130 detected in the reference location across the hippocampus (Figure 2a-b) and built an average
131 spatio-temporal propagation map per session (Figure 2c). Strong and common ripples in the

132 medial section showed a divergent propagation pattern: strong ripples travelling
133 medio→laterally and common ripples travelling in the opposite direction (Figure 2d-e). Ripples
134 detected in the lateral section did not show such strikingly divergent propagation (Figure 2f-
135 g) whereas, in the central section, the propagation was divergent only laterally and not
136 medially (Figure 2h-i). This peculiar propagation profile suggests a not previously described
137 underlying directionality along the hippocampal longitudinal axis and can be possibly
138 explained by a spatial bias in strong ripples generation. To understand the mechanism
139 underlying such difference in propagation we examined the location of the seed for each ripple
140 in sessions in which ripples were clearly detected in every hippocampal section (n sessions =
141 25). While we found no differences in the number of ripples detected in each hippocampal
142 section (p-value = 0.55, Kruskal-Wallis test), we observed differences regarding ripple
143 generation. In common ripples, regardless of the reference location, most ripples started from
144 the lateral section (Figure 3a left). On the other hand, strong ripples displayed a more
145 heterogenous picture (Figure 3a right). We identified two principles relative to strong ripples
146 generation: In all hippocampal sections the majority of strong ripples are locally generated,
147 and a greater number of strong ripples is generated medially than laterally. Looking at the
148 central section we can appreciate the difference between the number of strong ripples
149 generated medially and laterally (Figure 3a right, mean medial = $36.83 \pm 2.66\%$, mean lateral
150 = $20.55 \pm 2.04\%$, p-value = $3e-05$, Pairwise Tukey test). Strong and common ripples had
151 significantly different seed location profiles only in the medial and central section, not in the
152 lateral section (Figure 3b). These seed location profiles contribute to explain the propagation
153 idiosyncrasies: major unbalances in seeds location cause propagation patterns with clear
154 directionality, on the contrary, lag measurements hovering around zero are the result of
155 averaging between two similarly numbered groups of ripples with opposite direction of
156 propagation. Notably, propagation speed did not change depending on the seed location
157 (Supplementary Figure 4). The reason why strong ripples are only in a minority of cases
158 generated in the lateral section remains nevertheless unclear. Using a 'strength conservation
159 index' (SCI) we measured the ability of a ripple to retain its strength during propagation (a
160 ripple with SCI = 1 is in the top 10% in all hippocampal sections). We observed that ripples
161 generated laterally were effectively less able to retain their strength propagating towards the
162 medial pole (Supplementary Figure 5). This result is not simply explained by differences in
163 ripple strength along the medio-lateral (m-l) axis, as no such gradient was observed ($R^2 =$
164 0.0012, Supplementary Figure 6). Curiously, ripple amplitude showed a weak trend in the

165 opposite direction ($R^2 = 0.06$), with higher amplitude ripples in the lateral section
166 (Supplementary Figure 7).

167 **The hippocampal medial pole can generate longer ripples able to better engage neural** 168 **networks.**

169 To understand the reason behind the differential propagation we focused uniquely on the
170 central section, here it was possible to distinguish between ripples generated laterally or
171 medially ('lateral ripples' and 'medial ripples'). We included in the analysis sessions in which
172 ripples were clearly detected in each hippocampal section and with at least 100 ripples of
173 each kind (n sessions = 24). We looked at spiking activity associated with these two classes
174 of ripples in the hippocampal formation across the m-l axis (n clusters per session = $650.42 \pm$
175 33.16 , Figure 4a-b-c). To compare sessions, we created interpolated maps of the difference
176 between spiking induced by medial and lateral ripples (Figure 4d). Immediately following ripple
177 start (0-50 ms, "early phase") spiking was predictably influenced by ripple seed proximity: in
178 the lateral section lateral ripples induced more spiking (indicated by the blue color), whereas
179 in the medial section medial ripples dominated (indicated by the red color). Surprisingly, in the
180 50-120 ms window post ripple start ("late phase"), medial ripples could elicit significantly
181 higher spiking activity than lateral ripples along the entire m-l axis (Figure 4e). Dividing clusters
182 in putative excitatory and inhibitory using the waveform duration we observed the same effect
183 in both types of neurons (Supplementary Figure 8). In accordance with this result, we found
184 that the medial hippocampal section is able to generate longer ripples (Figure 4f). An important
185 portion of the variance in ripple duration is indeed explained by location on the m-l axis both
186 in common ($R^2 = 0.133$) and especially in strong ripples ($R^2 = 0.463$). The observed extended
187 spiking could be due to a increased number of neurons participating in the ripple, to a higher
188 spiking rate per neuron or a combination of these two elements. Fraction of active neurons
189 and spiking rate were both significantly higher in medial ripples (Supplementary Figure 9).
190 Focusing only on the late phase the difference in fraction of active neurons per ripples
191 between medial and lateral ripples was even more striking (Cohen's $d = 1.7$, Figure 4g).
192 Inversely, in the early phase, lateral ripples could engage more neurons, although, the effect
193 size was much smaller (Cohen's $d = 0.39$). The same result was found in relation to the spiking
194 rate, medial ripples caused a significant and considerable increase in spiking rate in the late
195 phase (Cohen's $d = 1.75$, Figure 4h). Dividing again the clusters into putative excitatory and
196 inhibitory, significant differences between medial and lateral ripples were present only in the
197 late phase. Spiking frequency and number of engaged neurons were significantly higher in

198 medial ripples both in putative excitatory and inhibitory clusters (Supplementary Figure 10). In
199 summary, the prolonged spiking observed in medial ripples was caused both by an increased
200 number of engaged neurons and a higher spiking rate per cell, both in putative excitatory and
201 inhibitory neurons. The disparity in network engagement can possibly be in part explained by
202 electrophysiological differences across hippocampal sections (e.g. higher firing rate). We did
203 not find differences in the number of firing neurons (medial = 74.73, lateral = 79.8, p-value =
204 3.56e-01, Mann-Whitney u test), we did, however, found differences in firing rate, waveform
205 duration, and waveform shape (recovery slope and peak-through ratio, Supplementary Figure
206 11). Firing rate and waveform duration exhibited respectively a left- and right-shifted
207 distribution in the lateral section, reflecting lower firing rate and slower action potentials.

208 **Discussion**

209 Our results show for the first time that strong ripples propagate differentially along the
210 hippocampal longitudinal axis. This propagation idiosyncrasy can be explained by a specific
211 ability of the hippocampal septal pole (medial section in our analysis) to produce longer ripples
212 that better entrain the hippocampal network and spread across the longitudinal axis. It was
213 previously observed that ripples located at the septal and temporal pole are generated
214 independently from each other, in addition, despite the presence of connections within the
215 hippocampal longitudinal axis (Witter, 2007, van Strien et al., 2009), in the vast majority of
216 cases ripples do not propagate to the opposite pole (Sosa et al., 2020). In accordance with
217 these results, we observed a strong effect of spatial distance on ripple strength correlation
218 confirming a previous study (Nitzan et al., 2022): the strength correlation, predictably, was
219 higher in CA1 pairs closer to each other. The effect of distance was also apparent on the ripple
220 chance of propagation, only half of the ripples generated in the septal pole were detected
221 additionally in the intermediate hippocampus (lateral section in our analysis). This chance is
222 much higher compared to the ~3.7% reported regarding propagation between opposite poles
223 (Sosa et al., 2020), it would be interesting to understand whether the temporal pole is also
224 able to entrain the intermediate hippocampus in similar fashion or it is a peculiarity of the
225 septal pole. A limitation of our work derives from the dataset being limited to the septal and
226 intermediate hippocampus, therefore we could not answer this question.
227 Ripples can arise at any location along the hippocampal longitudinal axis (Patel et al., 2013).
228 Our analysis shows that ripples are, however, not homogeneously generated across space.
229 We observed important differences between strong ripples and common ripples generation.

Common ripples followed a gradient with higher likelihood in the intermediate section and lowest in the septal pole. Strong ripples, on the other hand, are generated mostly locally (i.e. a strong ripple detected in the medial section is most likely generated in the medial section itself). Furthermore, only rarely a strong ripple generated in the intermediate hippocampus is able to propagate towards the septal pole retaining its strong status (top 10%). Conversely strong ripples generated in the septal pole have a significantly higher chance of propagate longitudinally and still be in the top 10% in terms of ripple strength. Notably, this is not consequence of a simple longitudinal gradient in ripple strength, indeed, we did not observe any difference in ripple strength along the longitudinal axis. Additionally, we show that ripples generated in the septal pole and in the intermediate hippocampus have a significantly different ability to engage hippocampal networks in the 50-120 ms window post ripple start. Ripples generated in the septal pole activate more neurons, both excitatory and inhibitory, and, moreover, elicit an higher spiking rate per neuron. This prolonged network activation is reflected by the fact that the position on the longitudinal axis explains 13.3% and 46.3% of the variability in ripple duration in common and strong ripples respectively. Consistent with a duration gradient along the longitudinal axis, the temporal hippocampus has been shown to produce shorter ripples both in awake and sleep conditions (Sosa et al., 2020). What is the reason that enables the septal pole to generate longer ripples? There might be for example underlying electrophysiological differences between the septal and intermediate hippocampus. Looking at units electrophysiological features we found some differences in the waveform shape and duration. We can hypothesize that slower action potentials and, consequentially, longer refractory periods hinder the ability to sustain protracted high frequency spiking. Accordingly, we found an increased firing rate and a smaller waveform duration in the septal pole. This might contribute to explain the prolonged ripples observed in the septal pole. We can also speculate that the neuromodulatory inputs gradient, monoamine fibers have been shown to be stronger in the ventral part (Strange et al., 2014), might influence neurons responses. Serotonin (ul Haq et al., 2016, Wang et al., 2015), noradrenaline (Ul Haq et al., 2012, Novitskaya et al., 2016) and acetylcholine (Zhang et al., 2021) have all been shown to suppress ripples. In accordance with this, some ripples are coupled with a reduced activation of the locus coeruleus and the dorsal raphe nucleus in vivo (Ramirez-Villegas et al., 2015).

Ripples can be subdivided in different types according to the relationship between the hippocampal LFP and the ripple itself (Ramirez-Villegas et al., 2015). Intriguingly these subtypes are associated with two different brain-wide networks, the first communicating

264 preferentially with the associative neocortex and a second one biased towards subcortical
265 structures. Moreover, these different types of ripples have been proposed to possibly fulfill
266 different functional roles. Given the different input/output connectivity between septal,
267 intermediate and temporal hippocampus (Fanselow and Dong, 2010) we hypothesize that
268 ripple generated at different points of the hippocampal longitudinal axis might as well have
269 functional differences, with the longer ripples generated septally possibly able to combine the
270 different kind of informations processed in the distinct hippocampal sections and additionally
271 relaying the integrated information back to the neocortex in accordance with the two-stage
272 memory hypothesis (Diekelmann and Born, 2010, Marr, 1971, Buzsáki, 1989, Rasch and Born,
273 2007, McClelland et al., 1995).
274 Long duration ripples have been shown to be of particular importance in situations of high-
275 memory demand (Fernández-Ruiz et al., 2019), at the same time, previous studies highlighted
276 the role of septal hippocampus in memory tasks and information processing (Hock and
277 Bunsey, 1998, Moser et al., 1993, Moser et al., 1995, Steffenach et al., 2005, Kheirbek et al.,
278 2013, McGlinchey and Aston-Jones, 2018, Fanselow and Dong, 2010, Maras et al., 2014,
279 Bradfield et al., 2020, Qin et al., 2020). Our results can contribute to explain the specific role
280 of septal hippocampus in memory-demanding tasks with its ability of generating particularly
281 long ripples that are able to strongly engage networks in the entire top half of the hippocampal
282 formation for an extended time.

283 **Materials and Methods**

284 **Dataset**

285 Our analysis was based on the Visual Coding - Neuropixels dataset provided by the Allen
286 Institute and available at
287 https://allensdk.readthedocs.io/en/latest/visual_coding_neuropixels.html. We excluded one
288 session (session id = 743475441) because of an artifact in the LFP time series (time was not
289 monotonically increasing). Two other sessions (session ids = 746083955, 756029989) were
290 excluded because of duplicated LFP traces. Other 6 sessions were excluded because of
291 absence of recording electrodes in CA1 (session ids=732592105, 737581020, 739448407,
292 742951821, 760693773, 762120172). Our analysis was therefore focused on 49 sessions,
293 average animal age = 119.22 ± 1.81 . Sex: males $n = 38$, females $n = 11$. Genotypes: wt/wt n
294 = 26, Sst-IRES-Cre/wt;Ai32(RCL-ChR2(H134R)_EYFP)/wt $n = 10$, Vip-IRES-Cre/wt;Ai32(RCL-
295 ChR2(H134R)_EYFP)/wt $n = 7$, Pvalb-IRES-Cre/wt;Ai32(RCL-ChR2(H134R)_EYFP)/wt $n = 6$.
296 Average probe count per session = 5.73 ± 0.08 . Average number of recording channels per
297 session = 2129.45 ± 29.46 . Probes in each session were numbered according to the position
298 on the M-L axis, with probe number 0 being the most medial. Channels with ambiguous area
299 annotations were discarded (e.g. HPF instead of CA1). We found a number of small artifacts
300 in a variety of sessions, all this timepoints were excluded from the analysis (for more
301 informations: https://github.com/RobertoDF/Allen_visual_dataset_artifacts). Further details
302 about data acquisition can be found at [https://brainmapportal-live-4cc80a57cd6e400d854-
303 f7fdcae.divio-media.net/filer_public/80/75/8075a100-ca64-429a-b39a-
304 569121b612b2/neuropixels_visual_coding_-_white_paper_v10.pdf](https://brainmapportal-live-4cc80a57cd6e400d854-f7fdcae.divio-media.net/filer_public/80/75/8075a100-ca64-429a-b39a-569121b612b2/neuropixels_visual_coding_-_white_paper_v10.pdf). Visualization of recording
305 locations was performed with brainrender (Claudi et al., 2021).

306 **Ripples detection**

307 The LFP traces sampled at 1250 Hz were filtered using a 6th order Butterworth bandpass filter
308 between 120.0 and 250.0. Ripples were detected on CA1 LFP traces, the best channel (higher
309 ripple strength) was selected by looking at the SD of the envelope of the filtered trace, if
310 multiple SD peaks were present across space (possibly caused by sharp waves in stratum
311 radiatum and ripple activity in stratum pyramidale) we subsequently looked at the channel
312 with higher skewness, in this way we could reliably identify the best ripple channel. The
313 envelope of the filtered trace was calculated using the Hilbert transform (`scipy.signal.hilbert`).
314 Ripple threshold was set at 5 SDs. Start and stop times were calculated using a 2 SDs

315 threshold on the smoothed envelope with window = 5 (`pandas.DataFrame.rolling`) to account
316 for ripple phase distortions. Ripple duration was limited at > 0.015 s and < 0.25 s. Candidate
317 ripples were excluded if preceded by another ripple in a window of 0.05 s. We estimated
318 power density of each candidate using a periodogram with constant detrending
319 (`scipy.signal.periodogram`) on the raw LFP trace, we checked the presence of a peak > 100
320 Hz, candidates not fulfilling this condition were discarded, this condition was meant to reduce
321 the number of detected false positives. Ripple candidates detected during running epochs
322 were discarded, an animal was considered to be running if his standardized speed was higher
323 than the 10th percentile plus 0.06. Candidates were also discarded if no behavioral data was
324 available. Code for the detection of ripples resides in 'Calculate_ripples.py'.

325 **Correlation and lag analysis**

326 In each session we uniquely used ripples from the CA1 channel with the strongest ripple
327 activity, we looked at the LFP activity in all brain areas recorded in a window of 100.0 ms pre
328 ripple start and 200.0 ms post ripple start, this broad windows account for possible travelling
329 delays due to distance. For each brain area we picked the channel with higher SD of the
330 envelope of the filtered trace. For each ripple considered we calculated integral of the
331 envelope of the filtered trace (J_{Ripple}) and the integral of the raw LFP (ripple-induced voltage
332 deflection, RIVD). After discarding channels with weak ripple activity (envelope variance < 5),
333 we computed the pairwise pearson correlation of the envelope traces of CA1 channels
334 (`pandas.DataFrame.corr`). For the lag analysis we first identified pairs of CA1 that satisfied a
335 distance requirements. Distance threshold were set at 25% ($857.29 \mu\text{m}$) and 75% (2126.66
336 μm) of the totality of distances. For each ripple detected in the reference channel we identified
337 the nearest neighbour in the other channel. The analysis was repeated after dividing ripples in
338 strong (top 10% J_{Ripple}) and common ripples (all remaining ripples) per session. Code for the
339 correlation and lag analysis resides in 'Calculations_Figure_1.py'.

340 **Ripple spatio-temporal propagation maps and ripple seed analysis**

341 The hippocampus was divided in three section with equal number of recordings. Channels
342 with weak ripple activity (envelope variance < 5) were discarded. Sessions with recording
343 locations only in one hippocampal sections or with less than 1000 ripples in the channel with
344 strongest ripple activity were discarded as well. For each ripple detected on the reference
345 CA1 channel we identified ripples in other CA1 channels happening in a window of ± 60.0 ms,
346 this events were grouped together in a 'cluster'. If more than one event was detected on the

347 same probe we kept only the first event. 'Clusters' were subsequently divided according to
348]Ripple on the reference electrode in strong and common ripples. Lag maps were result of
349 averaging lags for each probe. Code for the calculations of propagation maps resides in
350 'Calculate_trajectories.py'.

351 **Ripple-associated spiking activity**

352 We focused on sessions with clear ripple activity (envelope variance > 5) in all three
353 hippocampal sections and at least 100 ripples generated both medially and laterally. The
354 reference was always placed in the central section, here it was possible to identify ripples
355 generated medially and laterally. We only considered ripples that were detected in at least half
356 of the recording electrodes (in the code: "spatial engagment" > 0.5). For each ripple we
357 computed a histogram of spiking activity of regions belonging to the hippocampal formation
358 (HPF) in a window of 0.5 s centered on the ripple start in each probe. We averaged all the
359 computed histograms to create a spatial profile of spiking activity. To compare spiking activity
360 between sessions we interpolated (xarray.DataArray.interp) the difference between medial
361 ripples-induced spiking and lateral ripples-induced spiking over space (this was necessary
362 because probes in each sessions have different M-L coordinates) and time. We calculated the
363 number of active cells (at least one spike) and spiking rate of each cluster per ripple in a
364 window of 0.12 s starting from ripple start. We repeated the analysis separating the 0-50 ms
365 and 50-120 ms post ripple start windows.

366 **Units selection and features calculations**

367 Clusters were filtered according to the following parameters: Waveform peak-trough ratio <
368 5, ISI violations < 0.5, amplitude cutoff < 0.1 and Presence ratio > 0.1. For an explanation of
369 the parameters see
370 [https://github.com/AllenInstitute/ecephys_spike_sorting/blob/master/ecephys_spike_sorting](https://github.com/AllenInstitute/ecephys_spike_sorting/blob/master/ecephys_spike_sorting/modules/quality_metrics/README.md)
371 [/modules/quality_metrics/README.md](https://github.com/AllenInstitute/ecephys_spike_sorting/blob/master/ecephys_spike_sorting/modules/quality_metrics/README.md) and [https://brainmapportal-live-](https://brainmapportal-live-4cc80a57cd6e400d854-f7fdcae.divio-media.net/filer_public/80/75/8075a100-ca64-429a-b39a-569121b612b2/neuropixels_visual_coding_-_white_paper_v10.pdf)
372 [4cc80a57cd6e400d854-f7fdcae.divio-media.net/filer_public/80/75/8075a100-ca64-429a-](https://brainmapportal-live-4cc80a57cd6e400d854-f7fdcae.divio-media.net/filer_public/80/75/8075a100-ca64-429a-b39a-569121b612b2/neuropixels_visual_coding_-_white_paper_v10.pdf)
373 [b39a-569121b612b2/neuropixels_visual_coding_-_white_paper_v10.pdf](https://brainmapportal-live-4cc80a57cd6e400d854-f7fdcae.divio-media.net/filer_public/80/75/8075a100-ca64-429a-b39a-569121b612b2/neuropixels_visual_coding_-_white_paper_v10.pdf). Firing rate was
374 calculated on all clusters with presence ratio > 0.1.

375 **Acknowledgements**

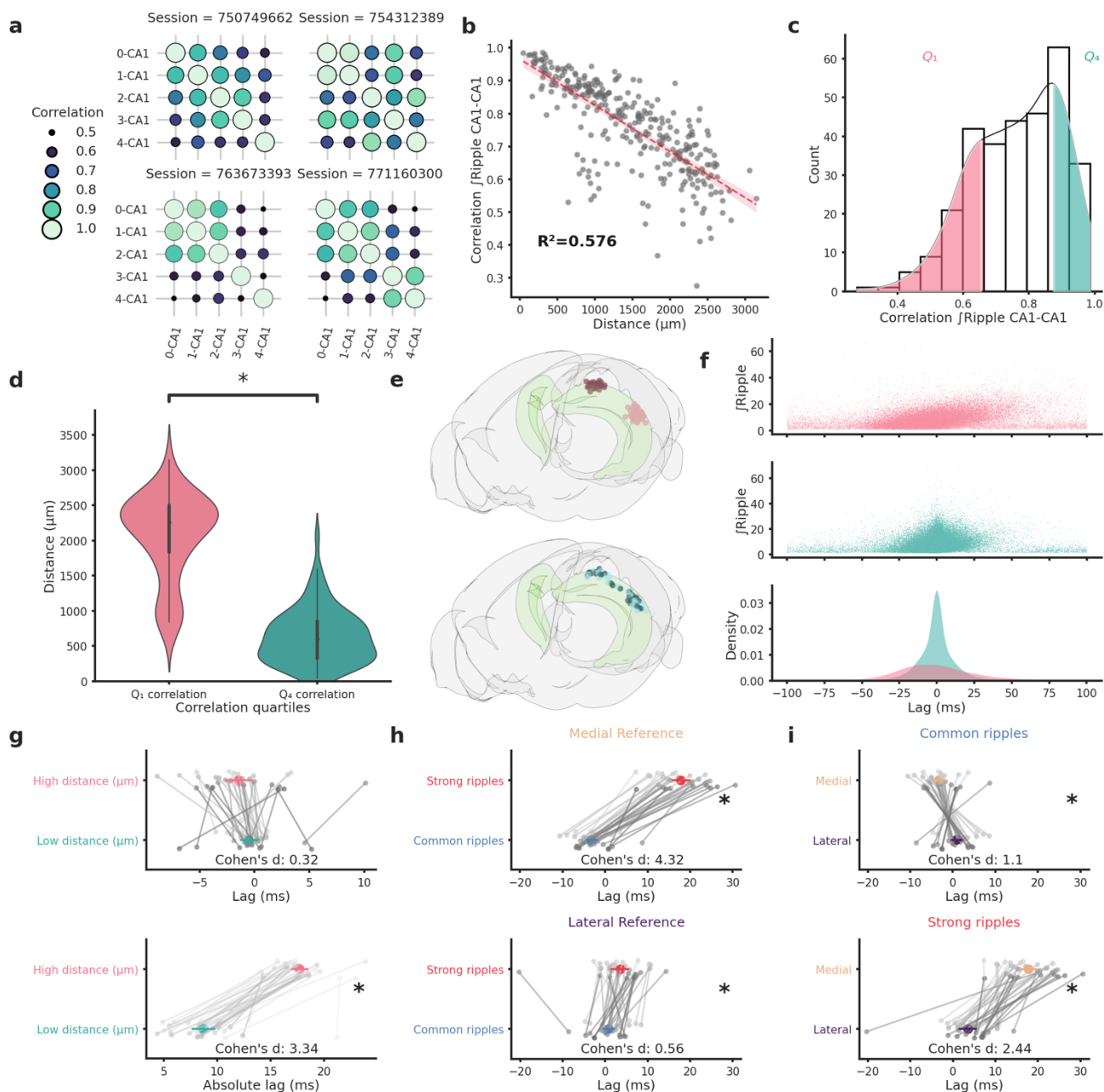
376 This study was supported by the German Research Foundation Deutsche
377 Forschungsgemeinschaft (DFG), project 184695641 - SFB 958, project 327654276 - SFB
378 1315, Germany's Excellence Strategy - Exc-2049-390688087) and by the European Research
379 Council (ERC) under the European Union's Horizon 2020 research and innovation programme
380 (Grant agreement No. 810580). We thank J.T. Tukker, N. Maier for feedback on an early
381 version of the manuscript and the members of the Schmitz lab for scientific discussion. We
382 thank Willy Schiegel and Tiziano Zito for technical help with cluster computing. We thank
383 Federico Claudi for support with brainrender. The authors declare that they have no
384 competing interests.

385 **Contributions**

386 Conceptualization, data curation, formal analysis, investigation, visualization: RDF. Writing -
387 original draft: RDF. Writing - review & editing: RDF, DS. Funding acquisition: DS.

388 **Data and materials availability**

389 All the code used to process the dataset is available at [https://github.com/RobertoDF/De-](https://github.com/RobertoDF/De-Filippo-et-al-2022)
390 [Filippo-et-al-2022](https://github.com/RobertoDF/De-Filippo-et-al-2022), pre-computed data structures can be downloaded at
391 [10.6084/m9.figshare.20209913](https://doi.org/10.6084/m9.figshare.20209913). All figures and text can be reproduced using code present in
392 this repository, each number present in the text is directly linked to a python data structure.
393 The original dataset is provided by the Allen Institute and available at
394 https://allensdk.readthedocs.io/en/latest/visual_coding_neuropixels.html.



396
 397 **Figure 1. Ripple strength correlation depends significantly on distance.**

398 (a) Correlation matrices showing the variability of ripple strength correlation between pairs of
 399 recording sites located in different CA1 locations in 4 example sessions. The number on the
 400 x and y axis labels indicates the probe number. Probes are numbered according to the
 401 position on the hippocampal longitudinal axis (0 is the most medial probe). (b) Scatter plot
 402 and linear regression showing the relationship between distance and correlation strength.
 403 Distance between recording sites explains 0.576% of the variability in correlation of ripple
 404 strength. (c) Ripple strength correlation distribution. Pink represents bottom 25% ($< q_1$) and
 405 blue top 25% ($> q_4$). (d) Violinplots showing that the top and bottom correlation quartile show

406 significantly different distance distributions (q_1 : $2077.57 \pm 68.68 \mu\text{m}$, q_4 : $633.56 \pm 44.02 \mu\text{m}$,
407 p -value = $4.00\text{e-}23$, Mann-Whitney u test). (e) Top: Rendering of the long distance (top) and
408 short distance (bottom) CA1 pairs, dark circles are the reference locations in each pair. (f) Top
409 and middle: scatter plots showing the relationship between ripple strength (at the reference
410 location) and lag for long distance (top, n ripples = 31855) and short distance (middle, n ripples
411 = 52858) pairs. Bottom: kernel density estimate of the lags of long distance (pink) and short
412 distance (turquoise) pairs. (g): Lag (top) and absolute lag (bottom) comparison between long
413 and short distance pairs (top: long distance = -1.47 ± 0.63 ms, Short distance = -0.51 ± 0.4
414 ms, p -value = $2.03\text{e-}01$, Student's t -test; bottom: long distance = 17.69 ± 0.38 ms, Short
415 distance = 8.69 ± 0.56 ms, p -value = $6.58\text{e-}20$, Student's t -test). (h) Lag comparison in long
416 distance pairs between common and strong ripples with reference located in the medial (top)
417 or lateral hippocampal section (bottom) (top: strong ripples = 17.83 ± 1.02 ms, common ripples
418 = -3.27 ± 0.68 ms, p -values = $2.28\text{e-}25$, Student's t -test, bottom: strong ripples = 3.62 ± 1.05
419 ms, common ripples = 0.88 ± 0.66 ms, p -values = $3.00\text{e-}02$, Student's t -test). (i) Lag
420 comparison in long distance pairs between ripples with reference located in the medial and
421 lateral section in common (top) or strong ripples (bottom) (top: medial reference = -3.27 ± 0.68
422 ms, lateral reference = 0.88 ± 0.66 ms, p -values = $4.30\text{e-}05$, Student's t -test, bottom: strong
423 ripples = 17.83 ± 1.02 ms, common ripples = 3.62 ± 1.05 ms, p -values = $4.30\text{e-}05$, Student's
424 t -test).

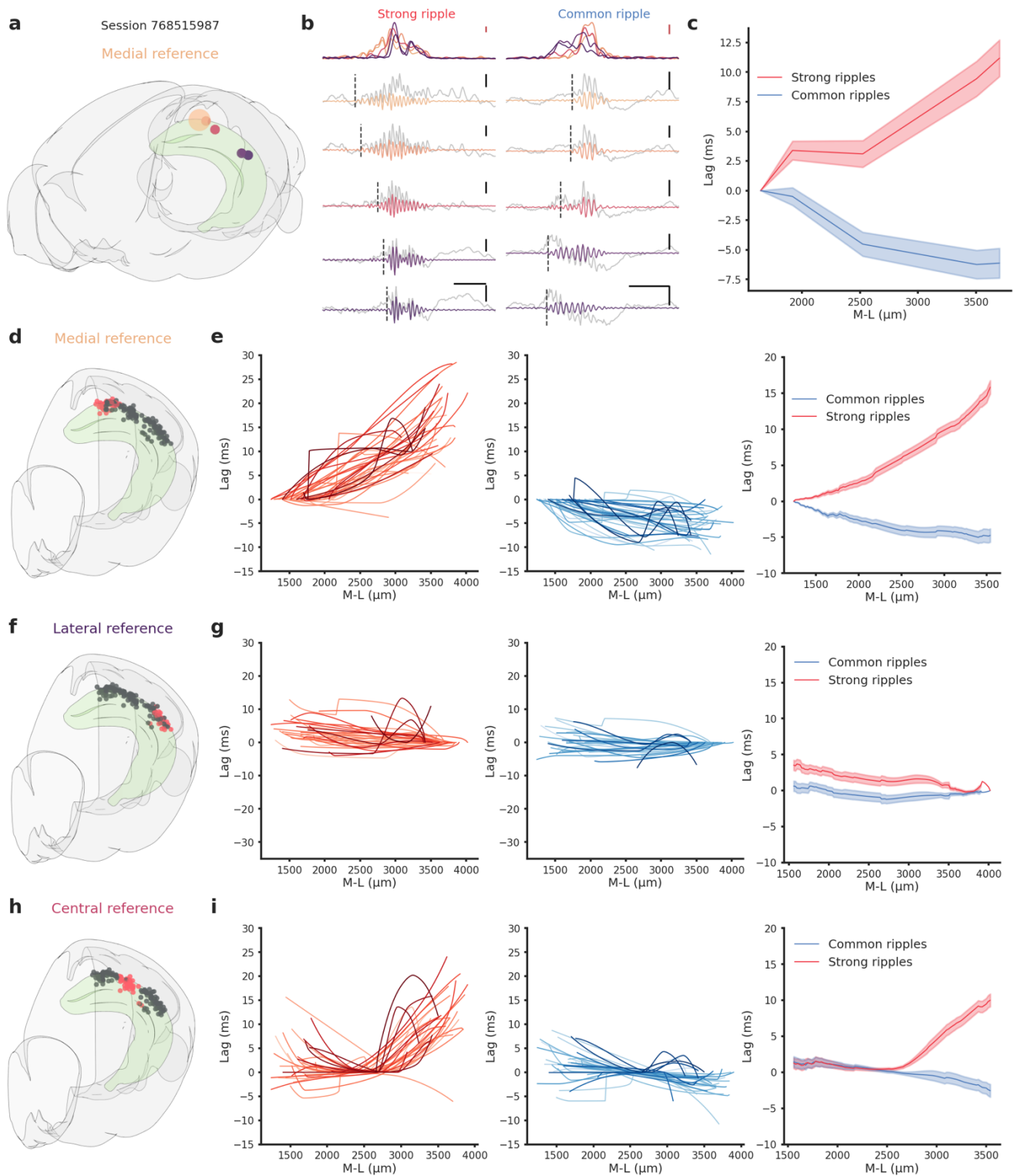


Figure 2. Direction-dependent differences in ripple propagation along the hippocampal longitudinal axis.

(a) Recording locations for session 768515987. Circles colors represents medio-lateral location. Bigger circle represents the reference location. (b) Example propagation of a strong (left column) and common (right column) ripple across the different recording location from session 768515987, each filtered ripple is color-coded according to a. Grey traces represents raw LFP signal. Dashed vertical line represents the start of the ripple. In the top row the ripple

433 envelope across all locations. Black scale bars: 50 ms, 0.5 mV. Red scale bars: 0.1 mV. (c)
434 Average propagation map of strong and common ripples in session 768515987 across the
435 medio-lateral axis. (d) Recording locations relative to e. Red circles represents the reference
436 locations across all sessions (n sessions=41), black circles represents the remaining recording
437 locations. (e) Left: Medio-lateral propagation of strong ripples, each line represents the
438 average of one session. Middle: Medio-lateral propagation of common ripples, each line
439 represents the average of one session. Right: Average propagation map across sessions of
440 strong and common ripples. Reference locations are the most lateral per session. (f) Same as
441 d. (g) Same as e. Reference locations are the most lateral per session. (h) Same as d. (i) Same
442 as e. Reference locations are the most central per session.

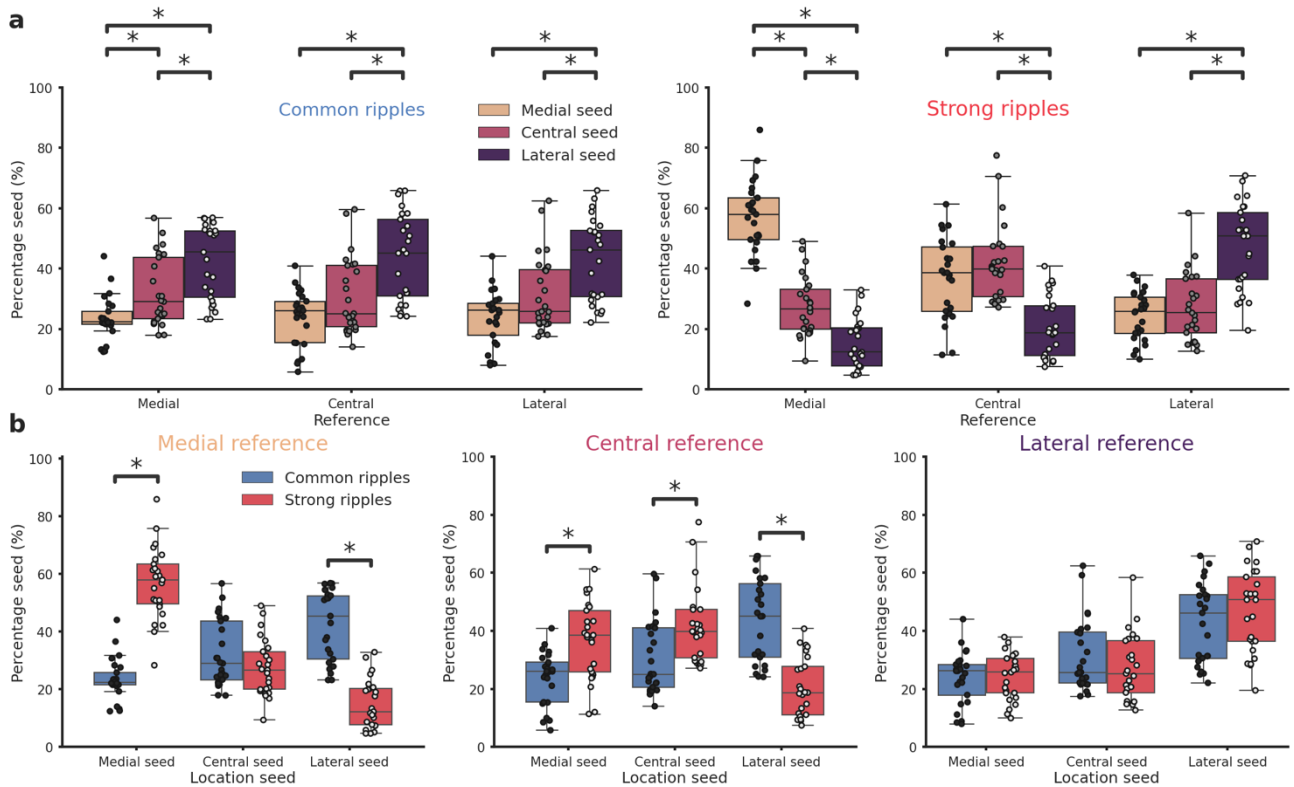


Figure 3. Ripples generation differences along the hippocampal longitudinal axis.

(a) Ripple seed location comparison between the three reference locations in common ripples (left) and strong ripples (right). Majority of common ripples seeds are located in the lateral hippocampal section regardless of the reference location (medial reference/lateral seed = 42.43 ± 2.45 %, central reference/lateral seed = 43.77 ± 2.9 %, lateral reference/lateral seed = 42.83 ± 2.75 %). Strong ripples are mainly local (medial reference/medial seed = 56.78 ± 2.48 %, central reference/central seed = 41.74 ± 2.58 %, lateral reference/lateral seed = 46.76 ± 2.89 %). (b) Ripple seed location comparison between strong and common ripples using a medial (left), central (center) or lateral reference (right). Asterisks mean $p < 0.05$, Kruskal-Wallis test with pairwise Mann-Whitney post-hoc test.

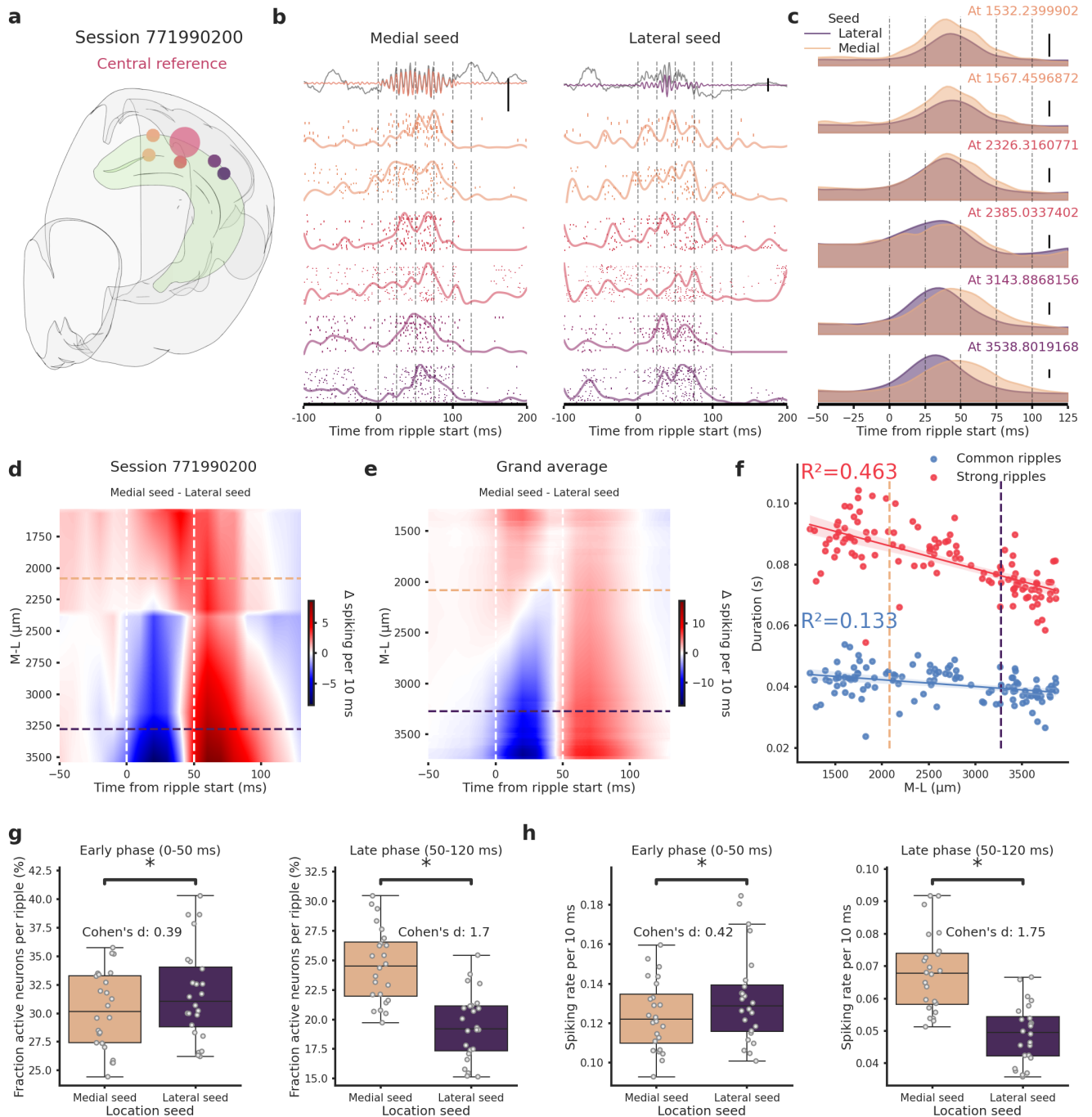


Figure 4. Ripples travelling in the medio→lateral direction show prolonged network engagement.

(a) Recording location for session 771990200. Circles colors indicate medio-lateral location. Bigger circle represents the reference location. (b) Spiking activity across the hippocampal m-l axis associated with a ripple generated medially (left column) or laterally (right column) across the different recording location from session 771990200. Spike raster plot and normalized density are plotted at each m-l location. In the top row filtered ripple, grey traces represents raw LFP signal. All plots are color coded according to a. Scale bar: 0.5 mV. (c) Kernel density estimates of the average spiking activity across different m-l locations and between seed type. Scale bar: 5 spikes per 10 ms. (d) Interpolated heatmap of the difference between medially

465 and laterally generated ripple induced spiking activity in session 771990200. Vertical dashed
466 lines represent borders between early and late post-ripple start phases. Horizontal dashed
467 lines represent the spatial limits of the hippocampal sections. (e) Grand average of the
468 differences between medially and laterally initiated ripple induced spiking activity across 24
469 sessions. Vertical dashed lines represent borders between early and late post-ripple start
470 phases. Horizontal dashed lines represent the spatial limits of the hippocampal sections. (f)
471 Regression plot between m-l location and ripple duration in common and strong ripples.
472 Horizontal dashed lines represent the spatial limits of the hippocampal sections. (g) Average
473 fraction of active neurons in medial (pink) and lateral (purple) ripples. Early/medial seed = 0.3
474 ± 0.69 , early/lateral seed: 31.72 ± 0.84 , p-value = $3.23\text{e-}05$, Student's t-test; late/medial seed
475 = 24.57 ± 0.64 , late/lateral seed = 19.44 ± 0.58 , p-value = $4.09\text{e-}07$, Student's t-test. (h)
476 Average spiking rate medial (pink) and lateral (purple) ripples. Early/medial seed = $0.12 \pm$
477 0.004 , early/lateral seed = 0.13 ± 0.005 , p-value = $1.35\text{e-}04$, Student's t-test; late/medial seed
478 = 0.07 ± 0.002 , late/lateral seed = 0.05 ± 0.002 , p-value = $1.24\text{e-}12$, Student's t-test.

479 BRADFIELD, L. A., LEUNG, B. K., BOLDT, S., LIANG, S. & BALLEINE, B. W. 2020. Goal-directed
480 actions transiently depend on dorsal hippocampus. *Nature Neuroscience*, 23, 1194-1197.

481 BUZSÁKI, G. 1989. Two-stage model of memory trace formation: a role for "noisy" brain states.
482 *Neuroscience*, 31, 551-70.

483 BUZSÁKI, G. 2015. Hippocampal sharp wave-ripple: A cognitive biomarker for episodic memory and
484 planning. *Hippocampus*, 25, 1073-188.

485 CARR, M. F., JADHAV, S. P. & FRANK, L. M. 2011. Hippocampal replay in the awake state: a
486 potential substrate for memory consolidation and retrieval. *Nat Neurosci*, 14, 147-53.

487 CLAUDI, F., TYSON, A. L., PETRUCCO, L., MARGRIE, T. W., PORTUGUES, R. & BRANCO, T.
488 2021. Visualizing anatomically registered data with brainrender. *eLife*, 10, e65751.

489 DAVIDSON, T. J., KLOOSTERMAN, F. & WILSON, M. A. 2009. Hippocampal replay of extended
490 experience. *Neuron*, 63, 497-507.

491 DIBA, K. & BUZSÁKI, G. 2007. Forward and reverse hippocampal place-cell sequences during ripples.
492 *Nat Neurosci*, 10, 1241-2.

493 DIEKELMANN, S. & BORN, J. 2010. The memory function of sleep. *Nature Reviews Neuroscience*,
494 11, 114-126.

495 DRAGOI, G. & TONEGAWA, S. 2011. Preplay of future place cell sequences by hippocampal cellular
496 assemblies. *Nature*, 469, 397-401.

497 FANSELOW, M. S. & DONG, H. W. 2010. Are the dorsal and ventral hippocampus functionally distinct
498 structures? *Neuron*, 65, 7-19.

499 FERNÁNDEZ-RUIZ, A., OLIVA, A., FERMINO DE OLIVEIRA, E., ROCHA-ALMEIDA, F.,
500 TINGLEY, D. & BUZSÁKI, G. 2019. Long-duration hippocampal sharp wave ripples improve
501 memory. *Science (New York, N.Y.)*, 364, 1082-1086.

502 FOSTER, D. J. & WILSON, M. A. 2006. Reverse replay of behavioural sequences in hippocampal place
503 cells during the awake state. *Nature*, 440, 680-3.

504 GIRARDEAU, G., BENCHENANE, K., WIENER, S. I., BUZSÁKI, G. & ZUGARO, M. B. 2009.
505 Selective suppression of hippocampal ripples impairs spatial memory. *Nat Neurosci*, 12, 1222-
506 3.

507 GIRARDEAU, G. & ZUGARO, M. 2011. Hippocampal ripples and memory consolidation. *Curr Opin*
508 *Neurobiol*, 21, 452-9.

509 HOCK, B. J., JR. & BUNSEY, M. D. 1998. Differential effects of dorsal and ventral hippocampal
510 lesions. *The Journal of neuroscience : the official journal of the Society for Neuroscience*, 18,
511 7027-7032.

512 HULSE, B. K., MOREAUX, L. C., LUBENOV, E. V. & SIAPAS, A. G. 2016. Membrane Potential
513 Dynamics of CA1 Pyramidal Neurons during Hippocampal Ripples in Awake Mice. *Neuron*, 89,
514 800-13.

515 JADHAV, S. P., KEMERE, C., GERMAN, P. W. & FRANK, L. M. 2012. Awake hippocampal sharp-
516 wave ripples support spatial memory. *Science*, 336, 1454-8.

517 KHEIRBEK, M. A., DREW, L. J., BURGHARDT, N. S., COSTANTINI, D. O., TANNENHOLZ, L.,
518 AHMARI, S. E., ZENG, H., FENTON, A. A. & HEN, R. 2013. Differential control of learning
519 and anxiety along the dorsoventral axis of the dentate gyrus. *Neuron*, 77, 955-968.

520 KUMAR, M. & DESHMUKH, S. S. 2020. Differential propagation of ripples along the proximodistal
521 and septotemporal axes of dorsal CA1 of rats. *Hippocampus*, 30, 970-986.

522 MARAS, P. M., MOLET, J., CHEN, Y., RICE, C., JI, S. G., SOLODKIN, A. & BARAM, T. Z. 2014.
523 Preferential loss of dorsal-hippocampus synapses underlies memory impairments provoked by
524 short, multimodal stress. *Mol Psychiatry*, 19, 811-22.

525 MARR, D. 1971. Simple memory: a theory for archicortex. *Philos Trans R Soc Lond B Biol Sci*, 262,
526 23-81.

527 MCCLELLAND, J. L., MCNAUGHTON, B. L. & O'REILLY, R. C. 1995. Why there are
528 complementary learning systems in the hippocampus and neocortex: insights from the successes
529 and failures of connectionist models of learning and memory. *Psychol Rev*, 102, 419-457.

530 MCGLINCHEY, E. M. & ASTON-JONES, G. 2018. Dorsal Hippocampus Drives Context-Induced
531 Cocaine Seeking via Inputs to Lateral Septum. *Neuropsychopharmacology*, 43, 987-1000.

532 MOSER, E., MOSER, M. & ANDERSEN, P. 1993. Spatial learning impairment parallels the magnitude
533 of dorsal hippocampal lesions, but is hardly present following ventral lesions. *The Journal of*
534 *Neuroscience*, 13, 3916-3925.

535 MOSER, M. B. & MOSER, E. I. 1998. Functional differentiation in the hippocampus. *Hippocampus*, 8,
536 608-19.

537 MOSER, M. B., MOSER, E. I., FORREST, E., ANDERSEN, P. & MORRIS, R. G. 1995. Spatial
538 learning with a minislabs in the dorsal hippocampus. *Proceedings of the National Academy of*
539 *Sciences*, 92, 9697-9701.

540 NITZAN, N., SWANSON, R., SCHMITZ, D. & BUZSÁKI, G. 2022. Brain-wide interactions during
541 hippocampal sharp wave ripples. *Proc Natl Acad Sci U S A*, 119, e2200931119.

542 NORMAN, Y., YEAGLE, E. M., KHUVIS, S., HAREL, M., MEHTA, A. D. & MALACH, R. 2019.
543 Hippocampal sharp-wave ripples linked to visual episodic recollection in humans. *Science*, 365,
544 eaax1030.

545 NOVITSKAYA, Y., SARA, S. J., LOGOTHETIS, N. K. & ESCHENKO, O. 2016. Ripple-triggered
546 stimulation of the locus coeruleus during post-learning sleep disrupts ripple/spindle coupling and
547 impairs memory consolidation. *Learn Mem*, 23, 238-48.

548 PATEL, J., SCHOMBURG, E. W., BERÉNYI, A., FUJISAWA, S. & BUZSÁKI, G. 2013. Local
549 generation and propagation of ripples along the septotemporal axis of the hippocampus. *J*
550 *Neurosci*, 33, 17029-41.

551 PFEIFFER, B. E. & FOSTER, D. J. 2015. PLACE CELLS. Autoassociative dynamics in the generation
552 of sequences of hippocampal place cells. *Science*, 349, 180-3.

553 QIN, C., BIAN, X.-L., WU, H.-Y., XIAN, J.-Y., CAI, C.-Y., LIN, Y.-H., ZHOU, Y., KOU, X.-L.,
554 CHANG, L., LUO, C.-X. & ZHU, D.-Y. 2020. Dorsal Hippocampus to Infralimbic Cortex
555 Circuit is Essential for the Recall of Extinction Memory. *Cerebral Cortex*, 31, 1707-1718.

556 RAMIREZ-VILLEGAS, J. F., LOGOTHETIS, N. K. & BESSERVE, M. 2015. Diversity of sharp-wave-
557 ripple LFP signatures reveals differentiated brain-wide dynamical events. *Proc Natl Acad Sci U*
558 *S A*, 112, E6379-87.

559 RASCH, B. & BORN, J. 2007. Maintaining memories by reactivation. *Curr Opin Neurobiol*, 17, 698-
560 703.

561 ROUX, L., HU, B., EICHLER, R., STARK, E. & BUZSÁKI, G. 2017. Sharp wave ripples during
562 learning stabilize the hippocampal spatial map. *Nat Neurosci*, 20, 845-853.

563 SIEGLE, J. H., JIA, X., DURAND, S., GALE, S., BENNETT, C., GRADDIS, N., HELLER, G.,
564 RAMIREZ, T. K., CHOI, H., LUVIANO, J. A., GROBLEWSKI, P. A., AHMED, R.,
565 ARKHIPOV, A., BERNARD, A., BILLEH, Y. N., BROWN, D., BUICE, M. A., CAIN, N.,
566 CALDEJON, S., CASAL, L., CHO, A., CHVILICEK, M., COX, T. C., DAI, K., DENMAN, D.
567 J., DE VRIES, S. E. J., DIETZMAN, R., ESPOSITO, L., FARRELL, C., FENG, D.,
568 GALBRAITH, J., GARRETT, M., GELFAND, E. C., HANCOCK, N., HARRIS, J. A.,
569 HOWARD, R., HU, B., HYTNEN, R., IYER, R., JESSETT, E., JOHNSON, K., KATO, I.,
570 KIGGINS, J., LAMBERT, S., LECOQ, J., LEDOCHOWITSCH, P., LEE, J. H., LEON, A., LI,
571 Y., LIANG, E., LONG, F., MACE, K., MELCHIOR, J., MILLMAN, D., MOLLENKOPF, T.,
572 NAYAN, C., NG, L., NGO, K., NGUYEN, T., NICOVICH, P. R., NORTH, K., OCKER, G. K.,
573 OLLERENSHAW, D., OLIVER, M., PACHITARIU, M., PERKINS, J., REDING, M., REID,
574 D., ROBERTSON, M., RONELLENFITCH, K., SEID, S., SLAUGHTERBECK, C.,
575 STOECKLIN, M., SULLIVAN, D., SUTTON, B., SWAPP, J., THOMPSON, C., TURNER, K.,
576 WAKEMAN, W., WHITESELL, J. D., WILLIAMS, D., WILLIFORD, A., YOUNG, R., ZENG,
577 H., NAYLOR, S., PHILLIPS, J. W., REID, R. C., MIHALAS, S., OLSEN, S. R. & KOCH, C.
578 2021. Survey of spiking in the mouse visual system reveals functional hierarchy. *Nature*, 592,
579 86-92.

580 SIROTA, A., CSICSVARI, J., BUHL, D. & BUZSÁKI, G. 2003. Communication between neocortex
581 and hippocampus during sleep in rodents. *Proc Natl Acad Sci U S A*, 100, 2065-9.

582 SOSA, M., JOO, H. R. & FRANK, L. M. 2020. Dorsal and Ventral Hippocampal Sharp-Wave Ripples
583 Activate Distinct Nucleus Accumbens Networks. *Neuron*, 105, 725-741.e8.

584 STEFFENACH, H. A., WITTER, M., MOSER, M. B. & MOSER, E. I. 2005. Spatial memory in the rat
585 requires the dorsolateral band of the entorhinal cortex. *Neuron*, 45, 301-13.

586 STRANGE, B. A., WITTER, M. P., LEIN, E. S. & MOSER, E. I. 2014. Functional organization of the
587 hippocampal longitudinal axis. *Nat Rev Neurosci*, 15, 655-69.

588 TAKAHASHI, S. 2015. Episodic-like memory trace in awake replay of hippocampal place cell activity
589 sequences. *Elife*, 4, e08105.

590 UL HAQ, R., ANDERSON, M. L., HOLLNAGEL, J.-O., WORSCHKECH, F., SHERKHELI, M. A.,
591 BEHRENS, C. J. & HEINEMANN, U. 2016. Serotonin dependent masking of hippocampal
592 sharp wave ripples. *Neuropharmacology*, 101, 188-203.

593 UL HAQ, R., LIOTTA, A., KOVACS, R., RÖSLER, A., JAROSCH, M. J., HEINEMANN, U. &
594 BEHRENS, C. J. 2012. Adrenergic modulation of sharp wave-ripple activity in rat hippocampal
595 slices. *Hippocampus*, 22, 516-533.

596 VAN STRIEN, N. M., CAPPAERT, N. L. & WITTER, M. P. 2009. The anatomy of memory: an
597 interactive overview of the parahippocampal-hippocampal network. *Nat Rev Neurosci*, 10, 272-
598 82.

599 VAZ, A. P., INATI, S. K., BRUNEL, N. & ZAGHLOUL, K. A. 2019. Coupled ripple oscillations
600 between the medial temporal lobe and neocortex retrieve human memory. *Science*, 363, 975-
601 978.

602 VOGEL, J. W., LA JOIE, R., GROTHE, M. J., DIAZ-PAPKOVICH, A., DOYLE, A., VACHON-
603 PRESSEAU, E., LEPAGE, C., VOS DE WAELE, R., THOMAS, R. A., ITURRIA-MEDINA, Y.,
604 BERNHARDT, B., RABINOVICI, G. D. & EVANS, A. C. 2020. A molecular gradient along
605 the longitudinal axis of the human hippocampus informs large-scale behavioral systems. *Nat*
606 *Commun*, 11, 960.

607 WANG, D., YAU, H.-J., BROKER, C., TSOU, J.-H., BONCI, A. & IKEMOTO, S. 2015. Mesopontine
608 median raphe regulates hippocampal ripple oscillation and memory consolidation. *Nature*
609 *neuroscience*, 18.

610 WITTER, M. P. 2007. Intrinsic and extrinsic wiring of CA3: indications for connectional heterogeneity.
611 *Learn Mem*, 14, 705-13.

612 XU, H., BARACKSKAY, P., O'NEILL, J. & CSICSVARI, J. 2019. Assembly Responses of Hippocampal
613 CA1 Place Cells Predict Learned Behavior in Goal-Directed Spatial Tasks on the Radial Eight-
614 Arm Maze. *Neuron*, 101, 119-132.e4.

615 YLINEN, A., BRAGIN, A., NÁDASDY, Z., JANDÓ, G., SZABÓ, I., SIK, A. & BUZSÁKI, G. 1995.
616 Sharp wave-associated high-frequency oscillation (200 Hz) in the intact hippocampus: network
617 and intracellular mechanisms. *J Neurosci*, 15, 30-46.

618 ZHANG, Y., CAO, L., VARGA, V., JING, M., KARADAS, M., LI, Y. & BUZSÁKI, G. 2021.
619 Cholinergic suppression of hippocampal sharp-wave ripples impairs working memory. *Proc Natl*
620 *Acad Sci U S A*, 118.